Bulletin of Engineering Geology and the Environment (2020) 79:3063–3073
https://doi.org/10.1007/s10064-020-01752-8

ORIGINAL PAPER

Experimental investigation and constitutive modeling of the shear creep behavior of an overconsolidated soft clay

Pan Ding[1] · Riqing Xu[1,2] · Yayuan Hu[1] · Jiaqi Xie[1] · Luying Ju[1]

Received: 13 December 2019 / Accepted: 17 February 2020 / Published online: 4 March 2020

Abstract

This paper presents the results of shear creep experimental investigations carried out on Huzhou overconsolidated soft clay and subsequently proposes a constitutive model that is able to reproduce the shear creep characteristics under complex stress conditions. First, shear creep characteristics are obtained based on the analysis of results from drained triaxial shear creep tests conducted on clay samples. Then, the Yin-Graham equivalent time is extended into shear stress states; thus, the concept of shear equivalent time is formulated. Using the shear creep characteristics observed from experiments and the shear equivalent time concept, a shear stress-strain-strain rate creep model reflecting a complex loading history and loading path is proposed. Finally, the model is solved numerically with the fourth-order Runge-Kutta method, and the predictions are compared with the measured values. The results show that (1) the shear creep coefficient of Huzhou overconsolidated soft clay varies with the overconsolidation ratio levels, and there is a good correspondence between them, which is similar to the relationship of the volumetric creep coefficient and overconsolidation ratio; (2) the predicted curves of the new model are in good agreement with measured curves, which demonstrates that the model can well simulate the shear creep characteristics of soft clay under complex stress conditions.

Keywords Overconsolidated soft clay · Shear creep tests · Constitutive model · Elastic-viscoplasticity · Equivalent time

Introduction

Soft clay is widely distributed in the southeast coastal area of China, where the economy is highly developed and the population is relatively dense. In parallel, large economic losses and human casualties are caused annually because of the post-construction settlement of engineering projects built on soft soil foundations, such as highways and high-speed railroads. Studies have shown that post-construction settlement on soft soil foundations is mainly caused by soil creep (Yao et al. 2018). Accordingly, studies of the creep behavior on soft soil foundations are of practical importance. In engineering practice, a technique combining surcharge loading and drainage consolidation has been widely used that can effectively reduce the magnitude of post-construction settlement (Bo et al. 2007; Lei et al. 2016; Wang et al. 2018).

The creep behaviors of geomaterials are usually classified as "volumetric creep" and "deviatoric creep" (Kavvadas and Kalos 2019; Venda Oliveira et al. 2019). In "volumetric creep", the dominant stress causing creep strains is isotropic stress, whereas the dominant stress in "deviatoric creep" is deviator stress. Moreover, deviatoric creep is also called shear creep in conventional triaxial states. The majority of studies are concentrated on volumetric creep behavior (Venda Oliveira et al. 2019), and scholars have performed tremendous work on laboratory studies and the modeling of volumetric creep behavior (Mesri and Castro 1987; Yin and Graham

✉ Yayuan Hu
huyayuan@zju.edu.cn

Pan Ding
Ding_pan@zju.edu.cn

Riqing Xu
xurq@zju.edu.cn

Jiaqi Xie
21512009@zju.edu.cn

Luying Ju
juluying0318@163.com

[1] Research Center of Coastal and Urban Geotechnical Engineering, Zhejiang University, Hangzhou 310058, China

[2] Zhejiang-California International Nano Systems Institute Taizhou Branch, Taizhou 318000, China

1999; Kim and Leroueil 2001; Zhou et al. 2018). In contrast, research on shear creep is relatively limited. In fact, shear creep can also lead to large accidents, such as shear deformation or the instability of steep slopes and the failure of shear zones in landslides (Li et al. 2019). Ma et al. (2014) conducted a set of shear creep tests on deep-sea simulative soil, and analyzed the creep strain characteristics under different shear stresses. Yang et al. (2012) applied the digital image processing technique to triaxial shear creep tests, and obtained more accurate experimental data for Shanghai muddy clay. These experimental studies have helped researchers to better understand the shear creep characteristics of soils, and provided a basis for further inductive theory building.

Regarding the modeling of the shear creep behavior of soils, scholars have developed a series of constitutive models (Singh and Mitchell 1968; Mesri et al. 1981; Borja 1992; Lai et al. 2014). The Singh-Mitchell model and Mesri model appear to be the most classical models. The Singh-Mitchell model gives reasonable predictions of creep strains for shear stress intensity in the range of 30–90%, but predictions at lower stress intensity are not satisfactory. To overcome this deficiency, Mesri et al. (1981) proposed a hyperbolic shear creep model with which to effectively describe the shear creep strains of soils under various stress levels. These two models are empirical models with few parameters, and give reliable predictions to some extent. However, these models have certain limitations, such as neglecting the influence of the overconsolidation ratio and adopting the real loading time, which make them unable to reflect the effects of the loading history and loading path.

Overconsolidated soil is formed due to the loading and reloading in the process of surcharge loading, and the overconsolidation ratio is the main cause affecting the behavior of overconsolidated soil. Gu et al. (2016) found through a series of experiments that the shear strength increased with increasing overconsolidation ratio OCR and suggested an equation to describe this phenomenon. Fujiwara and Ue (1990) and Leoni et al. (2008) pointed out that the settlements of overconsolidated soils depend greatly on the OCR value. In recent decades, much attention has been focused on the correlation of the secondary compression index ($C_{\alpha\varepsilon} = {}^{\triangle}\mathrm{e}/{}^{\triangle}\lg t$) or the volumetric creep coefficient ($C_{\alpha v} = {}^{\triangle}\varepsilon_v/{}^{\triangle}\lg t$) with other soil characteristics, such as the overconsolidation ratio (Ye et al. 2014). Mesri et al. (1997), Venda Oliveira et al. (2013), and Hu and Yang (2017) found that surcharge loading can effectively reduce the secondary consolidation coefficient of soils. Based on the tremendous analysis of experiments, Alonso et al. (2000) and Li et al. (2015, 2016) suggested that there is a one-to-one correspondence between the volumetric creep coefficient and OCR, and $C_{\alpha v}$ decreased with an increase in OCR. Lin and Wang (1998) combined Mesri's empirical rheological model with a power function of the OCR and deduced a shear creep constitutive model for overconsolidated soils. Wang and Peng (2006) further modified the stress-strain hyperbolic equation in Lin's model and formulated a shear creep model considering both strain-hardening and strain-softening phenomena simultaneously. The above two models did not establish an explicit relationship between the OCR and creep coefficient. That is, they failed to reflect the fact that the creep coefficient of overconsolidated soil varies with OCRs. Simultaneously, all of them were established using real loading time and failed to consider the influence of the loading path.

The "equivalent time method" suggested by Yin and Graham (1994) is an effective way to consider the influence of the loading path. Using the method, Yin and Graham deduced a general stress-strain-strain rate volumetric creep model. This model uses a logarithmic function with a constant creep coefficient to describe the creep compression, which is suitable for various loading paths. This work provides a promising method for considering the effects of the loading path and shines light on further studies.

Hence, in this research, a series of experiments was carried out on Huzhou soft clay to study the shear creep behavior of overconsolidated soil under complex loading conditions. Subsequently, using the creep characteristics observed from shear creep tests and the equivalent time concept, a shear creep model of overconsolidated soils is then derived. Finally, the analytical solutions for the model equation under fully drained conditions are obtained and verified through the experimental results of Huzhou soft clay.

Triaxial shear creep tests

Testing materials and methods

In this study, triaxial drained shear creep tests were conducted using a GDS automatic triaxial apparatus, which was designed and manufactured by the GDS corporation in the UK, and it can carry out conventional triaxial compression tests and creep tests under constant stress and stress relaxation tests under constant strain. A schematic diagram and photo of the apparatus are shown in Fig. 1. A typical schematic diagram of the controlling stress path is shown in Fig. 2 to elaborate the overall shear creep test processes. The soft clay studied herein was obtained from 5 to 9 m beneath the ground surface from the Huzhou region in China. This clay has high water contents, high compressibility, and low bearing capacity. The basic physical properties of these clay samples are listed in Table 1. To minimize soil disturbance and moisture loss, undisturbed soil samples were taken with a thin-walled tube sampler and sealed in metal tubes with the ends closed and transported to the laboratory. Finally, cylindrical specimens with a diameter of 39.1 mm and a height of 80 mm were carefully trimmed from the undisturbed soil and then mounted in the triaxial cell.

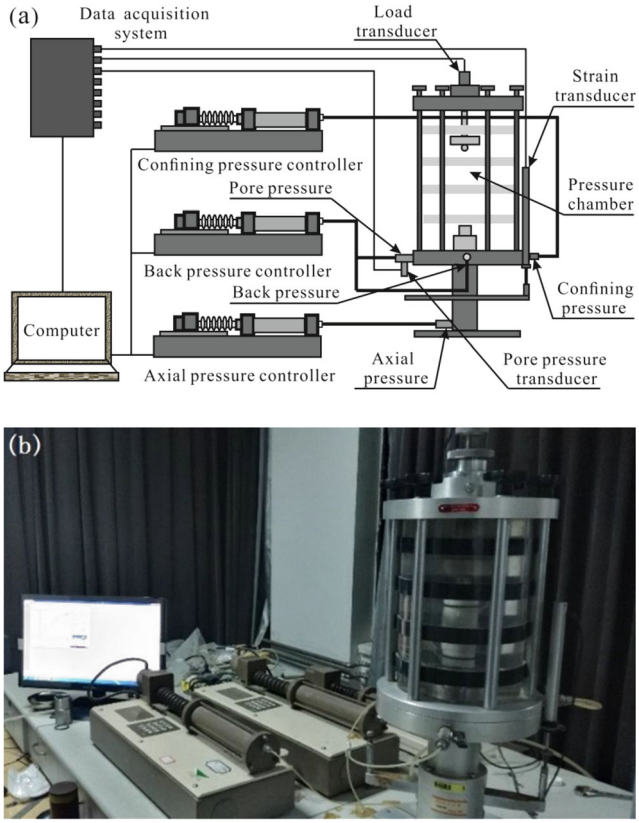

Fig. 1 GDS automatic triaxial apparatus: **a** sketch and **b** photo

Following this, a back pressure of 280 kPa with an effective stress of 20 kPa was applied (cell pressure equals 300 kPa), until B values greater than 0.98 were achieved, which indicates that the process of saturation is completed. This process usually took 20~30 h after the back pressure was applied.

After saturation, K_0 consolidation followed. In this process, the cell pressure is first increased with the back pressure unchanged to achieve the required effective confining pressure. Then, the axial pressure is gradually increased until the designed K_0 value is reached. The loading rate during these processes is 1 kPa/min.

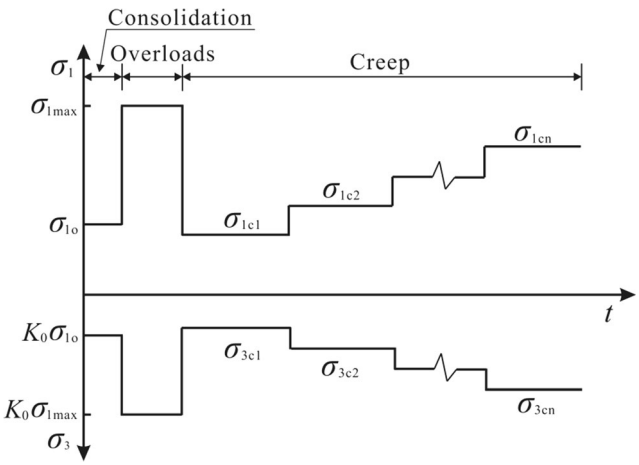

Fig. 2 Schematic diagram of the stress path

Table 1 Physical properties of Huzhou soft clays

ω(%)	ρ(g/cm^2)	G_s	ω_L(%)	ω_P(%)	c'(kPa)	φ'(°)
47.3	1.87	2.66	50.1	25.5	8.17	32.45

All the tests in this study were carried out under drained conditions, and the overconsolidation ratio is defined following the method suggested by Li et al. (2015), that is, using the shear stress to reflect the overconsolidation ratio.

$$\mathrm{OCR_q} = \frac{q_c}{q_0} \tag{1}$$

where $\mathrm{OCR_q}$ is the overconsolidation ratio defined by shear stress, which is also called the shear overconsolidation ratio; q_c is the pre-shear stress, or overloads; and q_0 is the current shear stress.

Based on the analysis of laboratory data from over 170 different soils, Mayne and Kulhawy (1982) investigated the relationship between K_0 and OCR and obtained an equation relating the two of them, which is expressed as $K_0 = K_{0nc}(\mathrm{OCR})^{\sin\varphi'}$ with $K_{0nc} = 1 - \sin\varphi'$. According to Mayne's work, K_0 increased with increasing OCR, which means that the K_0 coefficient of overconsolidated soils is larger than that of normally consolidated soils; other researchers also obtained similar conclusions (Sivakumar et al. 2009; Bozzano et al. 2014). The K_0 coefficient of Huzhou soft clays approximately equals 0.6, according to the above studies and former experiments. Therefore, in these experiments, specimens were initially K_0 consolidated up to σ_3' =30 kPa for a constant K_0 value of 0.6. After K_0 consolidation, the specimens were sheared to different overloads (40 kPa and 80 kPa). The specimens were then unloaded-reloaded to produce overconsolidated samples with specific $\mathrm{OCR_q}$ values. Once the desired $\mathrm{OCR_q}$ was reached, the specimen was allowed to creep for several days. The specific test scheme is shown in Table 2.

Test results and discussion

Figure 3a shows the test results between axial strains and elapsed time under five overconsolidation ratios (4.50, 3.00, 2.00, 1.33, and 0.89) on T1. Figure 3b shows the same curves under four overconsolidation ratios (4.00, 2.67, 1.78, and 1.19) on T2.

As shown in Fig. 3, Huzhou soft clay shows apparent creep behavior under the overconsolidation state. The relationships of axial strain ε_1 and elapsed time t are all power functions under different overconsolidation ratios. The axial strain increases rapidly with time in the initial loading phase, and

Table 2 Schemes of shear creep tests

Specimen	Consolidation pressure $(\sigma_1^{'},\sigma_3^{'})$/kPa	Overloads $(\sigma_1^{'}-\sigma_3^{'})_{max}$/kPa	Effective shear stress $(\sigma_1^{'}-\sigma_3^{'})$/kPa
T1	(50, 30)	40	20(1d) → 40(1d) → 8.9(3d) → 13.3(3d) → 20(3d) → 30(7d) → 45(5d)
T2		80	20(1d) → 80(1d) → 20(2d) → 30(2d) → 45(2d) → 67.5(2d)

evolves at a constant strain rate toward a stabilized state, corresponding to what is usually called primary and secondary creep stages (or called transient and stationary creep stages) (Augustesen et al. 2004; Andargoli et al. 2019); tertiary creep (or acceleration creep) behavior is not observed herein. It can also be found that the stable value of creep strain decreases with increasing overconsolidation ratio levels, which demonstrates that the surcharge preloading technique can effectively reduce the post-construction settlement of soft soil foundations.

Taking the natural logarithm of axial strain ε_1 and time t in Fig. 3, we obtain the $\ln\varepsilon_1$–$\ln t$ curves of different overconsolidation ratios for specimens T1 and T2, which are shown in Fig. 4 a and b, respectively.

Figure 4 shows that in the double-logarithmic coordinates, the axial strain increases linearly with the elapsed time. Unlike those of normally consolidated clay (Borja 1992), the straight lines herein are not parallel. The slope of these plots is the creep coefficient for shear creep tests, which is also called the shear creep coefficient λ.

$$\lambda = \frac{\Delta \ln \varepsilon_1}{\Delta \ln t} \tag{2}$$

The specific values of the shear creep coefficient λ of the two specimens are summarized in Table 3.

As shown in Table 3, for a given specimen, there is a negative correlation between the shear overconsolidated ratio

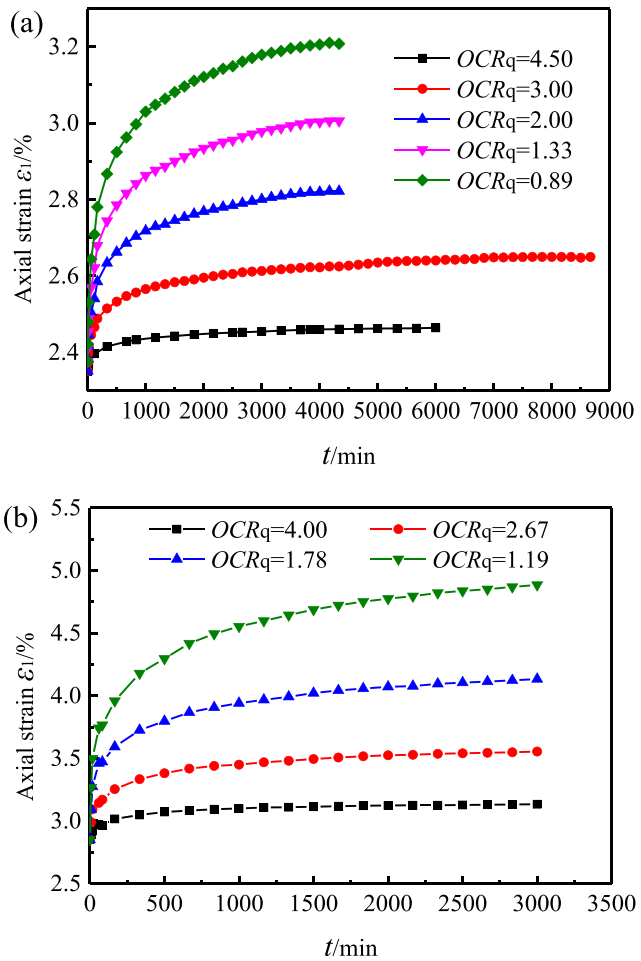

Fig. 3 Creep test results of ε_1 versus t of **a** specimen T1 and **b** specimen T2

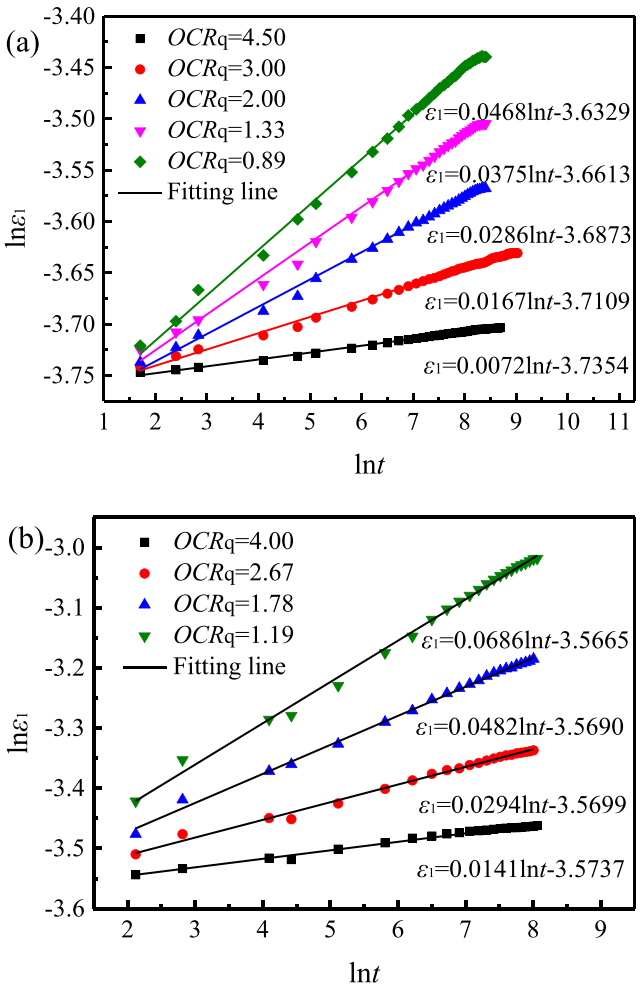

Fig. 4 Curves between $\ln\varepsilon_1$ and $\ln t$ of **a** specimen T1 and **b** specimen T2

Table 3 Shear creep coefficient of specimen T1 and T2

T1	OCRq	0.89	1.33	2	3	4.5
	λ	0.0468	0.0375	0.0286	0.0167	0.0072
T2	OCRq	1.19	1.78	2.67	4	
	λ	0.0686	0.0482	0.0294	0.0141	

OCR_q and shear creep coefficient λ. That is, an increase in OCR_q leads to a decrease in λ. To obtain the explicit equation of OCR_q and λ, the test data in Table 3 are plotted and fitted, and the fitting results corresponding to specimens T1 and T2 are shown in Fig. 5 a and b, respectively.

The fitting curves in Fig. 5 indicate that the shear creep coefficients of Huzhou soft clay under different overloads vary with OCR_q, and the mathematical formula can be written as

$$\lambda = A + B\exp\left(-C \times \mathrm{OCR}_q\right) \tag{3}$$

where A, B, and C are fitting parameters, and the specific values are shown in Table 4.

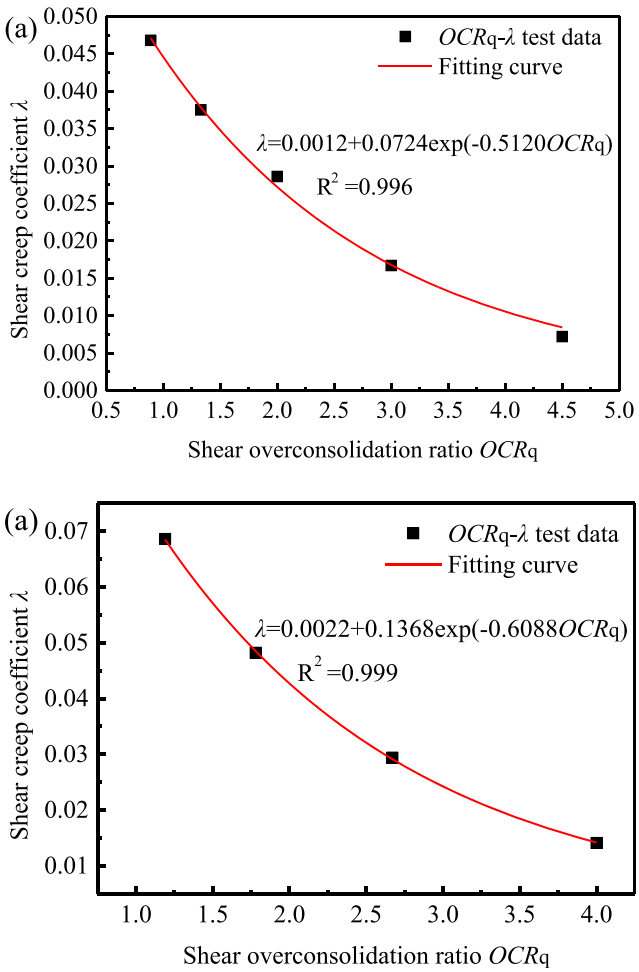

Fig. 5 Relationship curves between the shear creep coefficient and shear overconsolidation ratio of **a** specimen T1 and **b** specimen T2

It can be observed that the empirical formula of the shear creep coefficient versus the shear overconsolidation ratio is similar to that of the volumetric creep coefficient versus the overconsolidation ratio suggested by Alonso et al. (2000) or Li et al. (2015), which further verifies the rationality of the obtained empirical formula.

Shear creep model

To replicate the shear creep characteristics (such as the effects of loading history and loading path) observed in Huzhou overconsolidated soft soil, a more suitable constitutive model is needed.

Framework of the elastic viscoplastic model

Following the framework of Perzyna's overstress theory (Perzyna 1963, 1966), the total strain rate is decomposed into two parts: an elastic strain rate $\dot{\varepsilon}_1^{\mathrm{e}}$ and a viscoplastic strain rate $\dot{\varepsilon}_1^{\mathrm{vp}}$.

$$\dot{\varepsilon}_1 = \dot{\varepsilon}_1^{\mathrm{e}} + \dot{\varepsilon}_1^{\mathrm{vp}} \tag{4}$$

where ε_1 denotes the axial strain, a "dot" over the symbols indicates the rate of the variable, and the superscripts "e" and "vp" denote the elastic and viscoplastic components, respectively.

Generally, the elastic strain rate $\dot{\varepsilon}_1^{\mathrm{e}}$ can be written as

$$\dot{\varepsilon}_1^{\mathrm{e}} = \frac{\dot{p}'}{3K} + \frac{\dot{S}_1}{2G} \tag{5}$$

$$K = \frac{2(1+\nu)}{3(1-2\nu)}G \tag{6}$$

where p' denotes the effective mean normal stress; S_1 denotes the first deviator stress tensor, expressed as $S_1=\sigma_1'-p'$ in the generalized stress state (or $S_1=2\left(\sigma_1'-\sigma_3'\right)/3$ in the conventional triaxial state), where σ_1' and σ_3' denote the major and minor effective principal stresses, respectively; K and G denote the bulk modulus and shear modulus, respectively; and ν is Poisson's ratio, which usually takes the value of 0.3 for clays.

According to the theory of continuum thermomechanics with internal variables of state (Houlsby and Puzrin 2006; Maugin 2015), $\dot{\varepsilon}_1^{\mathrm{vp}}$ is a dissipative mechanical variable; in all generality, it is a function of the dissipative stress (shear stress q herein) and internal variable (axial strain ε_1 herein):

$$\dot{\varepsilon}_1^{\mathrm{vp}} = f(q, \varepsilon_1) \tag{7}$$

Equation (7) indicates that the viscoplastic strain rate $\varepsilon_1^{\mathrm{vp}}$ is related to shear stress q and axial strain ε_1. That is, for a given q and ε_1, the viscoplastic strain rate $\dot{\varepsilon}_1^{\mathrm{vp}}$ in relation to the (q, ε_1)

Table 4 Parameters of shear creep coefficient formulation

Overloads $(\sigma_1' - \sigma_3')_{max}$/kPa	Formula parameters		
	A	B	C
40	0.0012	0.0724	0.5120
80	0.0022	0.1368	0.6088

state is a certain value, which is independent of the way to reach the state. Therefore, the constitutive model related to the loading path can be established.

Shear equivalent time

Mesri et al. (1981) incorporated a power function of elapsed time into the Konder hyperbolic equation (Kondner 1963) and derived a stress-strain-time model for soils. As discussed previously, this model fails to reflect the effects of the loading path and loading history. Yin and Graham established a concept of equivalent time and derived a one-dimensional elastic viscoplastic model using the strain rate instead of real loading time. Referring to this concept, the effects of the loading path can be taken into consideration.

This section extends the equivalent time concept into shear stress states and makes preparations for further modeling.

As shown in Fig. 6, point i is the original state point, corresponding to a shear stress q_0 and a strain $\varepsilon_{1,i}$. The sudden application of a shear stress q_1 causes the path in (q, ε_1) space moves from point i to point $(i+1)'$ instantaneously, and then creep from point $(i+1)'$ to point $i+1$ under a constant stress q_1.

Similar to the definition of the Yin-Graham equivalent time, the shear equivalent time t_e is defined as the time needed to creep from the reference timeline to the current stress-strain (q, ε_1) state. The shear equivalent time of point i is $t_{e,i}$, corresponding to a unique stress-strain $(q_0, \varepsilon_{1,i})$ state. The shear equivalent time of point $(i+1)'$ is $t_{e,(i+1)'}$, which can be calculated from point i and the shear stress q_1. The shear

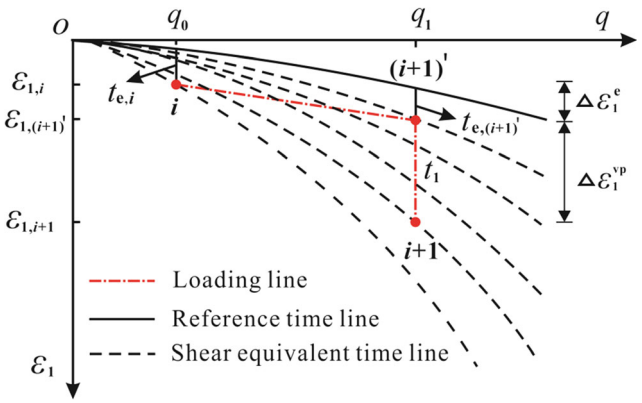

Fig. 6 Schematic diagram of the shear equivalent time

equivalent time of point $i+1$ can be expressed as the sum of $t_{e,(i+1)'}$ and real creep duration t_1. More details will be discussed later.

Formulation of a shear stress-strain-strain rate constitutive model

To consider the effects of the loading path, the Mesri creep model can be modified using equivalent time under conventional triaxial states ($\sigma_2' = \sigma_3'$, shear stress$q = \sigma_1' - \sigma_3'$)

$$\varepsilon_1 = \frac{1}{A_r}\frac{q}{1+B_r q}\left(\frac{t_r + t_e}{t_r}\right)^{\lambda} \tag{8}$$

where λ is the shear creep coefficient; t_r represents the reference time; t_e represents the equivalent time; and the hyperbolic parameters A_r and B_r correspond to the reference time t_r.

By calculating the derivative of Eq. (8) with respect to time, the stress-strain of the viscoplastic component can be derived as ($\dot{\varepsilon}_1^e = 0$ because stress remains constant during creep tests, so $\dot{\varepsilon}_1 = \dot{\varepsilon}^{vp}{}_1$)

$$\dot{\varepsilon}^{vp}{}_1 = \frac{\lambda}{A_r t_r}\frac{q}{1+B_r q}\left(\frac{t_r + t_e}{t_r}\right)^{\lambda-1} \tag{9}$$

As mentioned earlier, the shear creep coefficient λ is a function of the shear overconsolidation ratio OCR_q, which is expressed as Eq. (3) and simplified as

$$\lambda = \lambda(OCR_q) \tag{10}$$

Substituting Eq. (10) into Eq. (9) gives

$$\dot{\varepsilon}^{vp}{}_1 = \frac{\lambda(OCR_q)}{A_r t_r}\frac{q}{1+B_r q}\left(\frac{t_r + t_e}{t_r}\right)^{\lambda(OCR_q)-1} \tag{11}$$

Rearranging Eq. (8) leads to

$$t_e = -t_r + t_r\left[A_r\varepsilon_1\left(\frac{1}{q} + B_r\right)\right]^{\frac{1}{\lambda(OCR_q)}} \tag{12}$$

Substituting Eq. (12) into Eq. (11) gives

$$\dot{\varepsilon}^{vp}{}_1 = \frac{\lambda(OCR_q)}{t_r}\left[\frac{1}{A_r}\frac{q}{1+B_r q}\right]^{\frac{1}{\lambda(OCR_q)}}(\varepsilon_1)^{\frac{\lambda(OCR_q)-1}{\lambda(OCR_q)}} \tag{13}$$

It can be observed from Eq. (12) that time t_e is a function of shear stress and axial strain, which can be simplified as $t_e = f(q, \varepsilon_1)$. During the derivation of Eq. (13), t_e plays an important role as a bridge, transforming the stress-strain-time equation into the stress-strain-strain rates equation. Therefore, similar to Yin and Graham (1994, 1999), t_e is herein called the shear equivalent time.

As seen from Eq. (13), the viscoplastic strain rate is a unique function of three variables: shear stress q, axial strain ε_1, and shear overconsolidation ratio OCR_q, which makes it available for any loading path and loading history. That is, the viscoplastic strain rate $\dot{\varepsilon}_1^{vp}$ in relation to (q, ε_1, OCR_q) can be expressed and calculated by Eq. (13) in any loading condition.

Substituting Eqs. (5) and (13) into Eq. (4) yields

$$\dot{\varepsilon}_1 = \frac{\dot{p}'}{3K} + \frac{\dot{q}}{3G} + \frac{\lambda(\mathrm{OCR_q})}{t_r}\left[\frac{1}{A_r}\frac{q}{1+B_r q}\right]^{\frac{1}{\lambda(\mathrm{OCR_q})}}(\varepsilon_1)^{\frac{\lambda(\mathrm{OCR_q})-1}{\lambda(\mathrm{OCR_q})}} \quad (14)$$

Equation (14) is a shear stress-strain-strain rate relationship for overconsolidated clays that can simulate the effect of the loading path and loading history.

Solution for the creep model under fully drained conditions

To simulate the shear creep behavior of Huzhou soft clay, this section presents the solution for the above shear stress-strain-strain rate equation under fully drained conditions.

For a shear creep test under a certain OCR_q, the shear creep coefficient remains constant, which is set as λ_1 in the following part. The loading process of a shear creep test is shown in Fig. 6.

In drained conventional triaxial conditions, $p' = (\sigma_1' + 2\sigma_3')/3$, $q = (\sigma_1' - \sigma_3')$. The relation between the effective mean normal stress increment $\mathrm{d}p'$ and shear stress increment $\mathrm{d}q$ is given as (Xiao and Desai 2019)

$$\mathrm{d}p' = \mathrm{d}q/3 \quad (15)$$

Rewriting Eq. (14) into a differential form yields

$$\mathrm{d}\varepsilon_1 = \left(\frac{1}{9K} + \frac{1}{3G}\right)dq + \frac{\lambda_1}{t_r}\left[\frac{1}{A_r}\frac{q}{1+B_r q}\right]^{\frac{1}{\lambda_1}}(\varepsilon_1)^{\frac{\lambda_1-1}{\lambda_1}}\mathrm{d}t \quad (16)$$

The loading process from point i to point $i+1$ can be categorized into two stages: loading from point i to point $(i+1)'$ and loading from point $(i+1)'$ to point $i+1$.

The first stage is instantaneous ($t = 0$), so the corresponding viscoplastic strain equals 0. Integrating Eq. (16), gives

$$\int_{\varepsilon_{1,i}}^{\varepsilon_{1,(i+1)'}} \mathrm{d}\varepsilon_1 = \int_{q_0}^{q_1}\left(\frac{1}{9K} + \frac{1}{3G}\right)dq \quad (17)$$

Subsequently, the total strain $\varepsilon_{1,(i+1)'}$ in relation to point $(i+1)'$ can be written as

$$\varepsilon_{1,(i+1)'} = \varepsilon_{1,i} + \left(\frac{1}{9K} + \frac{1}{3G}\right)(q_1 - q_0) \quad (18)$$

The second stage is from point $(i+1)'$ to point $i+1$, and the creep duration is t_1. In this process, the shear stress remains constant at q_1, and only the viscoplastic strain is produced. Eq. (14) can be modified as

$$\dot{\varepsilon}_1 = \frac{\lambda_1}{t_r}\left[\frac{1}{A_r}\frac{q_1}{1+B_r q_1}\right]^{\frac{1}{\lambda_1}}(\varepsilon_1)^{\frac{\lambda_1-1}{\lambda_1}} \quad (19)$$

The whole process can be divided into n smaller processes, and can be expressed as $(i+1)', \cdots (i+1)^{j'}, \cdots (i+1)^{n'}$. The time duration of each tiny process becomes $\Delta t = t_1/n$, which is very short.

For the first process $(i+1)' \rightarrow (i+1)''$, the strain rate can be regarded as constant, and can be expressed by the rate at any point in this process (the front point $(i+1)'$ is selected herein).

According to Eq. (19), the strain rate of the first process can be written as

$$\dot{\varepsilon}_{1,(i+1)'} = \frac{\lambda_1}{t_r}\left[\frac{1}{A_r}\frac{q_1}{1+B_r q_1}\right]^{\frac{1}{\lambda_1}}\left(\varepsilon_{1,(i+1)'}\right)^{\frac{\lambda_1-1}{\lambda_1}} \quad (20)$$

the strain increment in this process is

$$\Delta\varepsilon_{1,1} = \dot{\varepsilon}_{1,(i+1)'}\Delta t = \frac{\lambda_1 t_1}{n t_r}\left[\frac{1}{A_r}\frac{q_1}{1+B_r q_1}\right]^{\frac{1}{\lambda_1}}\left(\varepsilon_{1,(i+1)'}\right)^{\frac{\lambda_1-1}{\lambda_1}} \quad (21)$$

Thus, the axial strain corresponding to point $(i+1)''$ is

$$\varepsilon_{1,(i+1)''} = \varepsilon_{1,(i+1)'} + \Delta\varepsilon_{1,1} = \varepsilon_{1,(i+1)'} + \dot{\varepsilon}_{1,(i+1)'}\Delta t \quad (22)$$

Substituting, Eqs. (18) and (21) into Eq. (22) results in

$$\varepsilon_{1,(i+1)''} = \varepsilon_{1,i} + \left(\frac{1}{9K} + \frac{1}{3G}\right)(q_1 - q_0) + \frac{\lambda_1 t_1}{n t_r}\left[\frac{1}{A_r}\frac{q_1}{1+B_r q_1}\right]^{\frac{1}{\lambda_1}}\left(\varepsilon_{1,(i+1)'}\right)^{\frac{\lambda_1-1}{\lambda_1}} \quad (23)$$

For the intermediate process $(i+1)^{j'} \rightarrow (i+1)^{j+1'}$, similar to the first process, the strain increment can be written as

$$\Delta\varepsilon_{1,j} = \dot{\varepsilon}_{1,(i+1)'}\Delta t = \frac{\lambda_1 t_1}{n t_r}\left[\frac{1}{A_r}\frac{q_1}{1+B_r q_1}\right]^{\frac{1}{\lambda_1}}\left(\varepsilon_{1,(i+1)'}\right)^{\frac{\lambda_1-1}{\lambda_1}} \quad (24)$$

The axial strain corresponding to point $i+1$ can be calculated by the sum of the strain increments of all n processes, which is

$$\varepsilon_{1,i+1} = \varepsilon_{1,(i+1)'} + \sum_j^n \Delta\varepsilon_{1,j} = \varepsilon_{1,i} + \left(\frac{1}{9K}+\frac{1}{3G}\right)(q_1 - q_0) + \sum_j^n \frac{\lambda_1 t_1}{n t_r}\left[\frac{1}{A_r}\frac{q_1}{1+B_r q_1}\right]^{\frac{1}{\lambda_1}}\left(\varepsilon_{1,(i+1)'}\right)^{\frac{\lambda_1-1}{\lambda_1}} \quad (25)$$

Once the soil parameters K, G, A_r, B_r, t_r, and λ are determined and the initial strain $\varepsilon_{1,i}$ as well as the corresponding shear stress q_0 are given, the shear creep strain at any point can be calculated by Eq. (25). For the sake of simplifying the calculation process, the whole procedure was programmed using the fourth-order Runge-Kutta method. Runge–Kutta methods are important methods for numerical integration of linear ordinary differential equations, with fair accuracy. Among them, the fourth-order Runge-Kutta method is the most classical with four stages. A general fourth-order Runge-Kutta method can be written as

$$\left.\begin{aligned} k_1 &= f(t_n, y_n)\\ k_2 &= f\left(t_n + \frac{h}{2}, y_n + \frac{h}{2}k_1\right)\\ k_3 &= f\left(t_n + \frac{h}{2}, y_n + \frac{h}{2}k_2\right)\\ k_4 &= f(t_n + h, y_n + hk_3) \end{aligned}\right\} \quad (26)$$

$$y_{n+1} = y_n + \frac{h}{6}(k_1 + 2k_2 + 2k_3 + k_4) \quad (27)$$

where $h = \Delta t$ is the time step, $t_n = nh$, and y_n is an approximation to $y(t_n)$.

To illustrate the implementation process of the Runge-Kutta method in the numerical program, a flowchart is shown in Fig. 7.

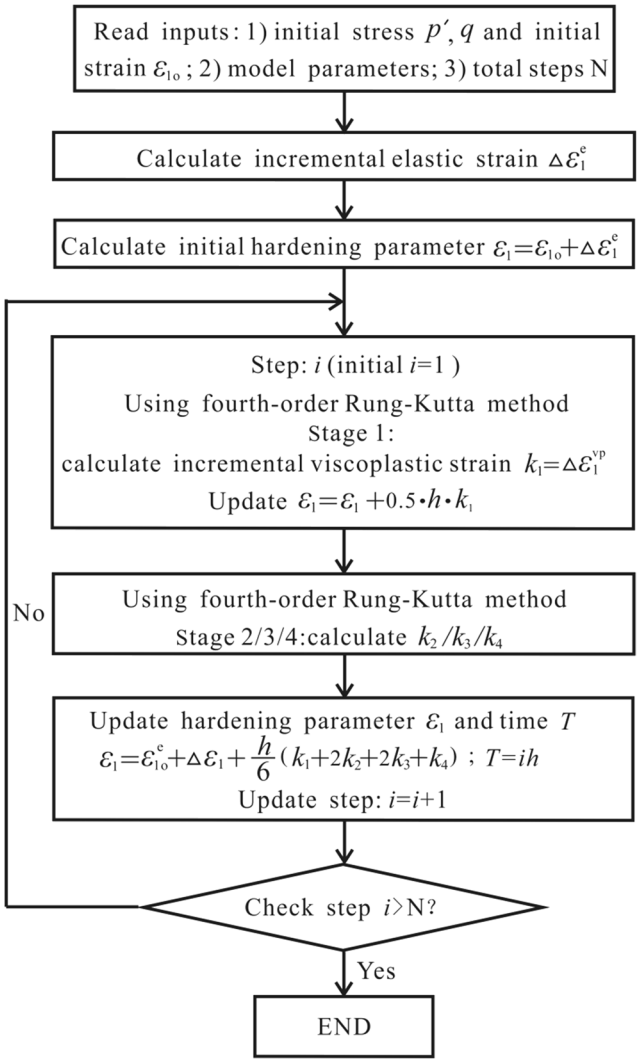

Fig. 7 Flowchart of the calculation program

Calibration and validation

Determination of model parameters

The parameters of the proposed shear creep model include shear modulus G, Poisson's ratio ν, reference time t_r, shear creep coefficient λ, and parameters A_r and B_r. All these parameters can be determined by a multistage shear creep test and conventional triaxial tests.

The shear modulus G can be determined by the unloading behavior of triaxial tests. It was found that G is a function of effective cell pressure σ_3', expressed as $G = G_0 p_a\left(\sigma_3'/p_a\right)^n$, the same as the equation given by Yang et al. (2019), where G_0 and n are fitting parameters; Poisson's ratio ν usually takes the default value of 0.3 for soft clays. Lin and Wang (1998) suggested that the reference time t_r can be selected arbitrarily because model parameters corresponding to different t_r can be converted to each other; t_r is chosen herein as 60 min (1 h); the shear creep coefficient λ is a function of OCR_q, which is expressed as Eq. (3).

The parameters A_r and B_r are determined as follows:

Rearranging Eq. (8) yields

$$\ln\varepsilon_1 = \ln(\varepsilon_{1o}) + \lambda\ln\left(\frac{t_r + t_e}{t_r}\right) \quad (28)$$

where

$$\varepsilon_{1o} = \frac{1}{A_r}\frac{q}{1+B_r q} \quad (29)$$

Rearranging Eq. (29) yields

$$\frac{1}{\varepsilon_{1o}} = A_r \frac{1}{q} + A_r B_r \tag{30}$$

Using the curve-fitting technique, parameters λ and ε_{1o} can be obtained in the $\ln\varepsilon_1$-$\ln[(t_r + t_e)/t_r]$ plot according to Eq. (28). The relationship of $\ln\varepsilon_{1o}$-$\ln[(t_r + t_e)/t_r]$ in drained triaxial creep tests for a constant q is almost linear. Therefore, parameters A_r and B_r can be obtained in the $1/\varepsilon_{1o}$-$1/q$ plot according to Eq. (30).

All parameters corresponding to Huzhou soft clay are determined using the above methods. The parameters for the shear creep coefficient are summarized in Table 4, and the other parameters are listed in Table 5.

The model parameters determination method used here is the deterministic method. Tan et al. (2018) pointed out that a deterministic method concerns the best fitting between the predictions and the observations, but ignores the uncertainties associated with statistical uncertainty, measurement error, and model uncertainty. The amount of measurement data may affect the accuracy of determining the model parameters, as do the unreasonable measurement data. However, as long as unreasonable measurement data are eliminated, the deterministic method is relatively simple with fair accuracy.

Validation of the model

According to the aforementioned solution method and soil parameters presented in Tables 4 and 5, the predictions of the proposed model are obtained numerically and compared with the experimental results. The comparisons are shown in Fig. 8.

Figure 8 a and b show the comparisons between the measured and simulated results for shear creep tests of specimens T1 and T2, respectively. In general, the predictions are all in reasonable agreement with the experimental results, although some discrepancies were noted (which may be caused by the uncertainty of the parameter determination method mentioned above), which indicates the accuracy of the new model. This model could also capture the basic shear creep behaviors as follows: (1) When the overload remains constant, the increment of strain decreases with increasing shear overconsolidation ratio levels. (2) The shear creep strains mainly occur in the initial stage of loading. With increasing loading time, the creep rate slows down, and the creep strain tends to be stable.

Table 5 Parameters of shear creep model

Overloads	G_0	n	ν	t_r/min	A_r/kPa	B_r/kPa^{-1}
40	15.15	0.937	0.3	60	43.14	0.8661
80	11.01	0.810	0.3	60	191.36	0.1280

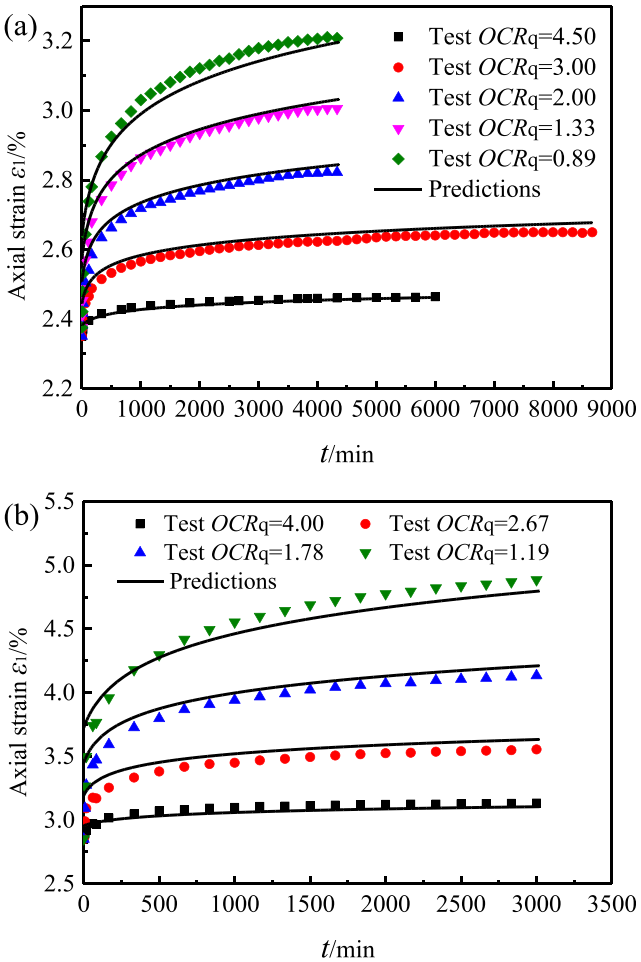

Fig. 8 Diagram between the shear strain and time of **a** specimen T1 and **b** specimen T2

Conclusions

In this study, the shear creep behaviors of Huzhou overconsolidated soft clays are investigated. A new shear stress-strain-strain rate model is then presented for simulating such behaviors. The following conclusions can be drawn.

(1) Similar to the relationship of the volumetric creep coefficient $C_{\alpha v}$ or secondary compression index $C_{\alpha e}$ versus the overconsolidation ratio OCR, there is a one-to-one correspondence between the shear creep coefficient λ and overconsolidation shear stress ratio OCRq. Moreover, λ decreases with increasing OCRq.

(2) The Yin-Graham equivalent time is extended into the shear stress state, and the concept of shear equivalent time is then established. With the extended shear equivalent time, the new model replaces the real loading time

with the strain rate and considers the influence of the overconsolidation ratio, which makes it possible to reflect the effects of the loading path and loading history.

(3) The solution of the model equation under drained conditions is obtained using the fourth-order Runge-Kutta method. Comparisons between the calculated results and test results indicate that the model is capable of predicting the shear creep behaviors of overconsolidated soft soils with fair accuracy.

The model is verified using shear creep tests, and further laboratory testing is suggested to verify the ability of this model in simulating other rheological behaviors, such as stress relaxation and strain rate effects.

Funding information The authors would like to acknowledge the financial support from the National Natural Science Foundation of China (Grant No. 41672264) and the Key Research and Development Program of Zhejiang Province (Grant No. 2019C03103).

Compliance with ethical standards

Conflict of interest The authors declare that they have no conflict of interest.

References

Alonso EE, Gens A, Lloret A (2000) Precompression design for secondary settlement reduction. Géotechnique 50(6):645–656

Andargoli MBE, Shahriar K, Ramezanzadeh A, Goshtasbi K (2019) The analysis of dates obtained from long-term creep tests to determine creep coefficients of rock salt. Bull Eng Geol Environ 78(3):1617–1629

Augustesen A, Liingaard M, Lade PV (2004) Evaluation of time-dependent behavior of soils. Int J Geomech 4(3):137–156

Bo MW, Arulrajah A, Nikraz H (2007) Preloading and prefabricated vertical drains design for foreshore land reclamation projects: a case study. Ground Improv 11(2):67–76

Borja RI (1992) Generalized creep and stress relaxation model for clays. J Geotech Eng 118(11):1765–1786

Bozzano F, Bretschneider A, Martino S, Prestininzi A (2014) Time variations of the K_0 coefficient in overconsolidated clays due to morphological evolution of slopes. Eng Geol 169:69–79

Fujiwara H, Ue S (1990) Effect of preloading on post-construction consolidation settlement of soft clay subjected to repeated loading. Soils Found 30(1):76–86

Gu C, Wang J, Cai YQ, Lei S, Wang P, Dong QY (2016) Deformation characteristics of overconsolidated clay sheared under constant and variable confining pressure. Soils Found 56(3):427–439

Houlsby GT, Puzrin AM (2006) Principles of hyperplasticity: an approach to plasticity theory based on thermodynamic principles. Springer verlag, London

Hu YY, Yang P (2017) Secondary settlement estimation in surcharge preload subject to time effect of secondary consolidation coefficient. J Cent South Univ 24(2):341–352

Kavvadas M, Kalos A (2019) A time-dependent plasticity model for structured soils (TMS) simulating drained tertiary creep. Comput Geotech 109:130–143

Kim YT, Leroueil S (2001) Modeling the viscoplastic behaviour of clays during consolidation: application to Berthierville clay in both laboratory and field conditions. Can Geotech J 38(3):484–497

Kondner RL (1963) Hyperbolic stress-strain response: cohesive soils. J Soil Mech Found 9(SM1):115–144

Lai XL, Wang SM, Ye WM, Cui YJ (2014) Experimental investigation on the creep behavior of an unsaturated clay. Can Geotech J 51(6):621–628

Lei HY, Wang XC, Chen L, Huang MS, Han J (2016) Compression characteristics of ultra-soft clays subjected to simulated staged preloading. KSCE J Civ Eng 20(2):718–728

Leoni M, Karstunen M, Vermeer PA (2008) Anisotropic creep model for soft soils. Géotechnique 58(3):215–226

Li GW, Huang K, Ruan YS, Li X, Yin JH (2015) The effect of principal stress ratio on creep behaviour of over-consolidated clay under plane strain conditions. Chin J Rock Mech Eng 34(12):2550–2558 (in Chinese)

Li GW, Li X, Ruan YS, Hou YZ, Yin JH (2016) Creep model of overconsolidated soft clay under plane strain. Chin J Rock Mech Eng 35(11):2307–2315 (in Chinese)

Li C, Tang H, Han D, Zou ZX (2019) Exploration of the creep properties of undisturbed shear zone soil of the Huangtupo landslide. Bull Eng Geol Environ 78(2):1237–1248

Lin HD, Wang CC (1998) Stress-strain-time function of clay. J Geotech Geoenviron Eng 124(4):289–296

Ma WB, Rao QH, Li P, Guo SC, Feng K (2014) Shear creep parameters of simulative soil for deep-sea sediment. J Cent South Univ 21(12):4682–4689

Maugin GA (2015) The saga of internal variables of state in continuum thermo-mechanics (1893–2013). Mech Res Commun 69:79–86

Mayne PW, Kulhawy FH (1982) K_0-*OCR* relationship in soil. J Geotech Eng Div ASCE 108(6):851–872

Mesri G, Castro A (1987) C_α/C_c concept and K_0 during secondary compression. J Geotech Eng 113(3):230–247

Mesri G, Rebres-Cordero E, Shields DR, Castro A (1981) Shear stress-strain-time behaviour of clays. Géotechnique 31:537–552

Mesri G, Stark TD, Ajlouni MA, Chen CS (1997) Secondary compression of peat with or without surcharging. J Geotech Geoenviron Eng 123(5):411–421

Perzyna P (1963) The constitutive equations for rate sensitive plastic materials. Q Appl Math 20(4):321–332

Perzyna P (1966) Fundamental problems in viscoplasticity. Adv Appl Mech 9:243–377

Singh A, Mitchell JK (1968) General stress-strain-time function for clay. J Soil Mech Found 94(SM1):21–46

Sivakumar V, Navaneethan T, Hughes D, Gallagher G (2009) An assessment of the earth pressure coefficient in overconsolidated clays. Geotechnique 59(10):825–838

Tan F, Zhou WH, Yuen KV (2018) Effect of loading duration on uncertainty in creep analysis of clay. Int J Numer Anal Methods Geomech 42(11):1235–1254

Venda Oliveira PJ, Correia AAS, Mira ESP (2013) Mitigation of creep deformations by preloading: laboratory study. Proc Inst Civ Eng (ICE) Geotech Eng 166(6):594–600

Venda Oliveira PJ, Santos SL, Correia AAS, Lemos LJL (2019) Numerical prediction of the creep behaviour of an embankment built on soft soils subjected to preloading. Comput Geotech 114:103140

Wang C, Peng Y (2006) A stress-strain-time function of saturated overconsolidated clay. Rock Soil Mech 27(S2):191–194 (in Chinese)

Wang J, Fang ZQ, Cai YQ, Chai JC, Wang P, Geng XY (2018) Preloading using fill surcharge and prefabricated vertical drains for an airport. Geotext Geomembr 46(5):575–585

Xiao Y, Desai CS (2019) Constitutive modeling for overconsolidated clays based on disturbed state concept. I: theory. Int J Geomech 19(9):04019101

Yang C, Wang R, Meng QS (2012) Study of soft soil triaxial shear creep test and model analysis. Rock Soil Mech 33(S1):105–111 (in Chinese)

Yang ZX, Xu TT, Li XS (2019) J2-deformation type model coupled with state dependent dilatancy. Comput Geotech 105:129–141

Yao YP, Qi SJ, Che LW, Chen J, Li MH, Ma XY (2018) Postconstruction settlement prediction of high embankment of Silty clay at Chengde airport based on one-dimensional creep analytical method: case study. Int J Geomech 18(7):05018004

Ye WM, Lai XL, Wang Q, Chen YG, Chen B, Cui YJ (2014) An experimental investigation on the secondary compression of unsaturated GMZ01 bentonite. Appl Clay Sci 97-98:104–109

Yin JH, Graham J (1994) Equivalent times and one-dimensional elastic viscoplastic modelling of time-dependent stress–strain behaviour of clays. Can Geotech J 31(1):42–52

Yin JH, Graham J (1999) Elastic viscoplastic modelling of the time-dependent stress-strain behaviour of soils. Can Geotech J 36(4): 736–745

Zhou WH, Tan F, Yuen KV (2018) Model updating and uncertainty analysis for creep behavior of soft soil. Comput Geotech 100:135–143